Slider Air Bearing Designs for Load/Unload Applications

Qing-Hua Zeng[1] and David B. Bogy

Computer Mechanics Laboratory,
Department of Mechanical Engineering,
University of California at Berkeley,
Berkeley, CA 94720

ABSTRACT

Dynamic load/unload (L/UL) has been widely used in portable drives, and it shows great potential in future high performance drives for avoiding slider-disk wear and stiction. Most current sliders are designed for contact-start-stop, and are not suitable for L/UL. In this paper, a previously introduced L/UL model for numerical simulation is improved. Four basic designs of air bearing surfaces with sub-ambient pressure cavities are presented, and their L/UL processes are simulated. We find that the ABS design significantly affects the L/UL performance. Two designs show very good unload performance – very small left-off force and short unload process, and the other two do not. We introduce a new slider, which meets all design and fabrication requirements, that has been designed specifically for L/UL. Further ways to improve its load performance are also discussed.

[1] Q. H. Zeng, Visiting researcher, Associate Professor, Institute of Vibration Engineering, Nanjing University of Aeronautics & Astronautics, China.

I. INTRODUCTION

Dynamic load/unload (L/UL) has been widely used in portable drives for achieving better shock resistance and lower power consumption. The disk drive industry is showing an increased interest in L/UL primarily for three applications. The first is for removable cartridge drives in which L/UL implemented by ramps is almost a standard mechanism. The second is the new generation of Winchester-type magnetic-optical drives, some using near-field recording, in which L/UL of the flying head is implemented to prevent media (plastic) damage. The third and most important is in fixed hard disk drives when L/UL is used to avoid wear and stiction, which are two major problems in current contact-start-stop (CSS) designs. Special landing zones based on laser texturing technology are widely applied in the industry. However, as the glide height decreases to provide high data densities, implementing effective landing zones is becoming more difficult. Therefore, L/UL is a good alternative to CSS, and it shows great potential for future high performance drives.

In disk drives, the air bearing sliders provide a small and steady spacing, flying height (FH), between the read/write sensors and the media. As the FH has decreased to increase the data density, many types of the sliders, with different air bearing surfaces (ABS) have been designed. The taper-flat slider is one of the simplest ABS designs, and it was widely used in the industry for about 15 years. To achieve the preferred performance, such as constant FH from the inner diameter (ID) to the out diameter (OD), low preload (normal load), high stiffness, steady FH, short settling time, altitude insensitivity, fast take-off, good contamination control, and lower manufacturing tolerance sensitivity, researchers have proposed many improved designs. For example, there are negative pressure sliders [1]-[3], transverse pressure contour sliders (TPC) [4], and shaped rail sliders with two or three rails [5], [6]. Combining these typical designs, researchers have proposed more complicated designs, such as the Headway AAB slider, the Seagate AAB slider [7], the tri-rail positive pressure and non-symmetric two-rail negative pressure sliders [8], and the

TNP slider [9]. There are also some special designs that are focused on special requirements, such as the tri-pad slider [10] for proximity recording, the contamination control slider [11], and the high damping slider [12] for good dynamics performance. However, most of these sliders were designed for CSS, and we found that few slider designs contain the desired features for L/UL, and therefore they are not suitable for L/UL applications. The sliders may contact the disk during L/UL. Even positive pressure sliders, which can generate sub-ambient pressure during unload because of skew effects, can possibly hit the disk during unload [13]. Therefore, it is time to study the design requirements and methods and to create some designs for L/UL applications.

In this paper, we study various ABS designs for L/UL by numerical simulation. A previously introduced L/UL model is improved. Four typical ABSs with sub-ambient cavities are designed, and their L/UL processes are simulated. We find that the ABS design significantly affects the L/UL performance of the sliders. Two ABS designs show very good L/UL performance, and the other two do not. Finally, we introduce a new slider, which meets all design and fabrication requirements, that is designed specifically for L/UL, and we illustrate its superior performance.

II. NUMERICAL MODEL AND SIMULATION

A. Slider Dynamics

The air bearing slider is attached to a suspension. Because of the constraints of the suspension, the slider's motion can be described as a system with three degrees of freedom (DOFs) by the following governing equations

$$m\frac{\mathrm{d}^2 z}{\mathrm{d}t^2} = -F_{sz} + F_{cz} + \iint_A (p - p_a)\mathrm{d}A \tag{1}$$

$$I_\theta \frac{\mathrm{d}^2 \theta}{\mathrm{d}t^2} = -M_{s\theta} + M_{c\theta} + \iint_A (p - p_a)(x_0 - x)\mathrm{d}A \tag{2}$$

$$I_\beta \frac{\mathrm{d}^2 \beta}{\mathrm{d}t^2} = -M_{s\beta} + M_{c\beta} + \iint_A (p - p_a)(y - y_0)\mathrm{d}A \tag{3}$$

In Eqs. (1)-(3), z, θ and β are the vertical displacement at the slider's center, and the slider's pitch and roll; m, I_θ and I_β are the mass and moments of inertia of the slider. F_{sz} is the suspension force in the Z-direction, $M_{s\theta}$ and $M_{s\beta}$ are suspension moments in the pitch and roll directions, p_a is ambient pressure, and p is the pressure governed by the generalized Reynolds equation. F_{cz} is the contact force, and $M_{c\theta}$ and $M_{c\beta}$ are the contact moments. The contact force and moments are approximately calculated by the elastic-plastic model [14].

The suspension is modeled as a spring/damper system, in which the suspension force applied on the slider in the Z-direction is

$$F_{sz} = \min\langle k_z\left[z + x_d * \sin(\theta) + y_d * \sin(\beta) - vt - z_0\right] + c_z\left[\dot{z} + x_d * \dot{\theta} + y_d * \dot{\beta} - v\right], \mathrm{F_{s0}}\rangle \quad (4)$$

and the suspension moments are

$$M_{s\theta} = M_{s\theta 0} + k_\theta \theta + c_\theta \dot{\theta} + x_d * F_{sz} \quad (5)$$

and

$$M_{s\beta} = M_{s\beta 0} + k_\beta \beta + c_\beta \dot{\beta} + y_d * F_{sz} \quad (6)$$

where k_z,, k_θ, k_β, c_z, c_θ, and c_β are stiffness and damping coefficients of the suspension in the Z, pitch and roll directions. F_{s0} is the normal load, and v is the L/UL speed. The applied location of the force can be changed by specifying the off-set x_d and y_d to the dimple in the X and Y directions. For the suspensions with a load dimple, suspension parameters can change during the L/UL process based on F_{sz}. If F_{sz}>0, the dimple is in contact, and x_d=0 and y_d=0. If F_{sz}<0, the dimple has separated, and x_d and y_d may have non zero values.

B. Suspension Modeling

The suspension parameters can be directly measured. But a better way is to calculate these parameters from a FE model of the suspension including the L/UL mechanism. The FE model is preliminarily verified by modal experiments [15], [16]. The HTI 850AK suspension was modified by attaching a load wire for L/UL. A FE model, shown in Fig.

1, was created and verified in its free state. The damper coefficients were estimated from the calculated slider inertia and the measured damping ratios of the first three modes. The stiffness coefficients were obtained from the FE model by fixing the load point at the load wire, applying a given force or moment at the slider center, and calculating the displacement or rotation of the slider. The offsets x_d and y_d can also be calculated from the FE model by fixing the four corners of the slider, applying a given force in the Z direction at the load point, and calculating the four reaction forces at the four corners. The offsets can be estimated from these four reaction forces. These parameters are shown in Table 1.

Substituting (4)-(6) into (1)-(3), and simultaneously solving the equations (1)-(3) and the generalized Reynolds equation, we can obtain the slider's response. Equations (1)-(3) are solved by using direct numerical integration. The CML dynamic load/unload simulator [13] was developed to implement the model by updating the CML Air Bearing Dynamic Simulator. This model has been previously used to simulate the first three stages of the unload processes of negative pressure sliders with no contact, and it was verified by experiments [17]. In this paper, we used the model to simulate the entire process of both load and unload. The contact at the dimple is modeled by discontinuous changes of the parameters.

III. AIR BEARING DESIGNS FOR L/UL

The simulations of many current popularly used sliders and some experimental data show that different ABS designs have very different L/UL performance. Some of these results were presented in [16], [17]. Problems exist in both the load and unload processes. During load, the sliders hit the disks for some initial conditions, such as negative pitch. The initial conditions are not fully controllable because the sliders vibrate during unload due to suspension flexibility and airflow excitation, so many sliders will hit the disks during load. During unload, the suction forces generated by sub-ambient cavities and/or

the effects of skew angle result in dimple separation and an extended unload process. For suspensions with no dimple or with a limitor to prevent dimple separation, the suction forces result in strong suspension oscillation and a long unload process. The long unload process will reduce the recordable area on the disks for L/UL ramps with desirable slopes. Therefore, better ABS designs are required to achieve good L/UL performance. Since negative pressure sliders have many merit features, we retain these features and improve their L/UL performances.

A. Four Basic Types of ABS Designs and Their Unload Performances

The design procedure is divided into two steps – optimization of the unload performance and then improvement of the load performance. Therefore, design objectives are to minimize the lift-off forces during UL and to prevent the slider from impacting the disk during load. The fixed design conditions are: 50% slider, two pads at the trailing edge, 5400 RPM, with the steady flying state at a 44 mm radius (0 skew) of 58 nm FH, 220 μrad pitch, 34.4 mN normal load and -58.9 mN suction force. The basic idea is to control the pitch angle during L/UL. We designed four basic types, which can represent many current sliders, based on different arrangements of the sub-ambient cavities that can control the pitch angle during L/UL. The ABSs of these sliders are shown in Fig.2. They have almost the same steady FHs, pitch and suction forces. The Type A slider has two cavities located on the sides of the slider from the leading to trailing edges, the Type B slider has one cavity near the leading edge, the Type C has one at the slider center, and the Type D has one cavity near the trailing edge. The forces during unload at 50 mm/s and 5400 RPM were calculated and are shown in Fig.2. We can see that the first two sliders have large lift-off forces (-18.87 mN and –22.65 mN) and longer unload processes (about 10.8 ms and 12.4 ms), and they therefore are not suitable for L/UL applications. The suction forces of these two sliders also result in large dimple separations (about 0.32 and 0.4 mm) and strong oscillations. On the other hand, the last two sliders have almost

no lift-off force and very short and stable unload processes (about 2.5 ms), and they may be suitable for L/UL applications.

Figure 3 shows the flying attitudes of the Type B slider during unload. The unload process can be divided into four stages. As shown in Figs.2b) and 3, in the first stages, the air bearing force decreases from the initial load (34.4 mN) to zero. The FH steadily increases from 58.7 nm to 143.6 nm, while the pitch changes from 217.5 urad to 248.9 urad. The positive pressure resultant force of the bearing decreases from 93.3 mN to 58 mN, and the suction force is almost constant at 58.9 mN. In the second stage, the air bearing force changes from 0 to a maximum negative value of –22.65 mN at 11.8 ms. The dimple separates, reaching the maximum separation of about 0.4 mm. The FH and pitch change from 143.6 nm to 424.9 nm and 248.9 urad to 587.9 urad, respectively. In the third stage, the air bearing quickly disappears in about 0.6 ms, while the FH and pitch sharply increase to 21.69 um and 0.19 rad, respectively. This occurs because the slider is pulled by the tensioned suspension springs. In the last stage, the slider strongly vibrates due to the combination effects of the slider inertia and suspension forces. First, the dimple closes, and the slider continues moving up and pushing up the loadbeam by the inertia effects of the slider. At the peak point, the load wire loses contact with the ramp. Then, the slider and loadbeam move down due to the effect of the loadbeam spring. Then, the dimple separates again because of the slider inertia effects. The slider approaches the disk, and it almost hits the disk at about 13.5 ms as shown in Fig. 3 b). Many simulation results show that the negative pressure sliders usually hit the disk during unload at the first or second dimple separation.

Figure 4 shows the flying attitudes of the Type D slider during unload. The unload process is significantly different from that of the Type B slider. In the first stage the air bearing force decreases from the initial load (34.4 mN) to zero. The FH steadily increases from 58.5 nm to 142.8 nm, while the pitch changes from 216.0 urad to 633.0 urad. The positive pressure resultant force of the bearing decreases from 93.9 mN to 40.3 mN, and

the suction force decreases from 59.5 mN to 40.3 mN. Comparing the Type D slider with the Type B slider we see that the major differences are the changes of the pitch and suction force. The change of pitch of the Type D slider is significant in the first stage, and thereby results in the decrease of the suction force and the smaller lift-off force. We almost cannot identify the second stage. After the air bearing disappears, the slider shows very small oscillations. The unload process is finished in 2.5 ms, which is only 20% of the time required for the Type B slider. It should be mentioned that the unload time is dependent not only on the ABS design, but also on the unload speed and the suspension stiffness. The larger the suspension stiffness, the shorter the unload time. A short unload time is important for increasing the recordable area and simplifying the L/UL mechanism design. One concern of the Type D slider might be the air bearing stiffness or normal load sensitivity. It is surprising that Type D has less sensitivity than Type B. For example, if the normal load changes from 34.4 mN (3.5 gram) to 29.43 mN (3.0 gram), the FH of Type D changes from 58.5 nm to 65.7 nm, while the FH of Type B changes from 58.7 nm to 67.9 nm. We also simulated the load processes of the four sliders, and found that the Type C and D sliders load smoother than the Type A and B.

B. A Slider Specifically Designed for L/UL Application

We found that the FH of the Type C slider is very sensitive to the disk speed, and it is difficult to achieve a constant FH from the ID to the OD. Therefore, the Type D slider was modified to meet the other design and fabrication requirements, such as constant FH at all radii, good contamination control, small roll angle (control of minimum FH), rail size (>300 um, for holding the read/write sensor), wall profile (25^{o}), recess (3 um) and taper (320 um, 10 μrad). The optimized slider is shown in Fig. 5. The slider has two small pads at the leading edge symmetrically arranged. There is a larger pad and a cavity near the trailing edge. They are asymmetric for achieving constant FH from the ID to the OD at the read/write sensor, which is located at (2.015 mm, 1.4 mm). The pressure profile at the ID is shown in Fig. 6. The steady flying attitudes at 5400 RPM are shown in Table 2.

The FH at the sensor is about 25.5 nm. We see that the FHs are almost identical from the ID to the OD. Moreover, the roll angles of the slider at the ID and the OD are very small, and thereby the slider has a relatively large minimum FH, which helps prevent slider-asperity contacts during the steady flying state. The FH is also shown in Table 2 for the normal load decreased from 34.4 mN to 29.43 mN.

The unload performances were evaluated in the RPM range from 1000 to 7000. Figure 7 shows the lift-off force and displacement histories during unload at the OD and 2000 RPM. The force and displacement histories are very similar to those shown in Fig. 2 d) at 5400 RPM. Figure 8 shows the lift-off force is a function of disk RPM. We see that the lift-off forces at higher RPM are very small, and this slider has very good unload performance at higher RPM, such as 5400 RPM.

The load performance of this slider was also evaluated in the RPM range from 2000 to 5400, for the four combinations of positive and negative pitch and roll (5 mrad) and with a 20 um initial FH at the slider's center for a 30 mm/s load speed. It was found that the worst initial condition is a negative pitch and positive roll. Figure 9 shows the FH at the leading edge-out rail, pitch, roll and air bearing force histories during load at 5400 RPM, and Figure 10 shows the same cases at 2000 RPM. We see that the slider contacts the disk at the leading edge-out rail, and then gradually settles down at 5400 RPM, however the slider can be smoothly loaded at 2000 RPM. The critical RPM is about 3500. The slider will contact the disk if it is loaded at more than 3500 RPM. That is because of a larger suction force at the high RPM when the slider has a negative pitch and positive roll. Furthermore, the suction force, with the profile shown in Fig. 11, will decrease the pitch angle and increase the roll, that further increases the suction force. Finally, the slider contacts the disk. Therefore, this slider has very good loading performance at the lower RPM.

We can improve its load performance at higher RPM by changing the ABS design. The basic idea is to keep the suction force as small as possible and the force center near the

center line and trailing edge at the worst load condition. After checking the pressure profile shown in Fig. 11, we redesigned the slider by combining the two small pads into one pad that is located at the center and near the leading edge. The redesigned slider, as shown in Fig. 12, has better load performance.

IV. CONCLUSIONS

The air bearing slider design for dynamic load/unload application was studied by numerical simulation. A previously introduced L/UL model was improved, and a procedure was described to obtain the suspension parameters that are used in the model. Four basic designs of ABS with sub-ambient pressure cavities were presented and their L/UL processes were simulated. We found that the ABS design significantly affects the L/UL performance. Two designs, with cavities near the slider center or the trailing edge, show very good unload performance, and the other two, with cavities from the leading to the trailing edge or near the leading edge, do not.

A new slider, which meets all design and fabrication requirements, has been designed specifically for L/UL applications. The slider has very good unload performance at higher disk RPM, and the preferred load performance at lower RPM. The design principle for L/UL sliders is to keep the negative pressure regions (not only the cavities) near the center line and trailing edge during the L/UL processes after considering the worst loading conditions and skew effects.

ACKNOWLEDGMENT

This study is supported by the Computer Mechanics Laboratory at the University of California at Berkeley. We thank Dr. C. Singh Bhatia, SSD/IBM, for helpful discussions on slider design constraints and fabrication requirements.

REFERENCES

[1] M. F. Garnier, T. Tang, and J. W. White, "Magnetic Head Slider Assembly," U.S. Patent No. 3,855,625, 1974.

[2] K. Kogure, S. Fukui, Y. Mitsuya, and R. Kaneko, "Design of Negative Pressure Slider for Magnetic Recording Disks", *ASME, J. of Lubrication Technology,* Vol. 105, pp. 496-502, 1993.

[3] J. W. White, "Flying Characteristics of the 'Zero-Load' Slider Bearing," *J. of Lubrication Technology*, Vol. 105, pp. 484-490, 1983.

[4] J. W. White, "The Transverse Pressure Contour Slider: Flying Characteristics and Comparison with Taper-Flat and Cross-Cut Type Sliders," *ASME, Adv. in Info. Storage Syst.,* Vol. 3, pp. 1-14, 1991.

[5] H. Nishihira, L. Dorius, and S. Bolasna, "Performance Characteristics of the IBM 3380K air bearing design," *Tribology and Mechanics of Magnetic Storage Systems*, 5, pp. 117-123, 1988.

[6] P. R. Peck, B. S. Wang, K. O. Park, and M. S. Jhon, "Scaling Criteria for Slider Miniaturization Including Shape Effects," *Proc. Sixth Intl. Symp. Adv. Infr. Storage Proc. System*, ISPS-Vol. 1, pp. 1-6, 1995.

[7] C. Hardie, A. Menon, P. Crane, and D. Egbert, "Analysis and Performance Characteristics of the Seagate Advanced Air Bearing Slider," *IEEE Tran. of Magnatics Vol.30*, pp. 424-432, 1994.

[8] D. S. Chhabra, S. A. Bolasna, L. K. Dorius, and L. S. Samuelson, “Air Bearing Design Considerations for Constant Fly Height Applications,” *IEEE Tran. of Magnatics Vol.30*, pp. 417-423, 1994.

[9] J. W. White, "Flying Characteristics of the Transverse and Negative Pressure Contour ('TNP") Slider Air Bearing," *ASME, J. of Tribology*, Vol. 119, pp. 241-248, 1996.

[10] C. M. Leung and N. V. Gitis, "Tri-pad Airbearing Technology,' *IEEE, Tran. of Magnatics*, Vol. 32, 1996.

[11] S. Zhang and D. B. Bogy, "Slider Designs for Controlling Contamination," *ASME, J. of Tribology*, Vol.119, pp. 537-540, 1997.

[12] Q. H. Zeng and D. B. Bogy, "Stiffness and Damping Evaluation of Air Bearing Sliders and New Designs with High Damping", *ASME, J. of Tribology*, (in press).

[13] Q. H. Zeng and D. B. Bogy, "The CML Dynamics Load/Unload Simulator (Version 421.10)," Technique report 98-08, Computer Mechanics Lab., Department of Mechanical Engineering, University of California at Berkeley, April, 1998.

[14] W. R. Chang, I. Etsion, and D. B. Bogy, "An Elastic-Plastic Model for the Contact of the Rough Surfaces," *ASME J. of Tribology*, Vol. 109, pp. 257-263, 1987.

[15] Q. H. Zeng and D. B. Bogy, "Dynamic Characteristics of a Suspension Assembly, Part 1: Modal Experiment," *ASME Advances in Information Storage System*, Vol. 8, 1997, (in press).

[16] Q. H. Zeng and D. B. Bogy, "Dynamic Characteristics of a Suspension Assembly, Part 2: Numerical Analysis," *ASME Advances in Information Storage System,* Vol. 8, 1997, (in press).

[17] Q. H. Zeng, M. Chapin, and D. B. Bogy, "Dynamics of the unload Process for Negative Pressure Sliders," Asia-Pacific Magnetic Recording Conf., Singapore, July, 1998 (submitted to *IEEE Tran. of Magnetics*).

TABLE 1 Suspension Parameters (N,m,rad,s)

Parameters	Dimple closed	Dimple open
k_z	276.5	48.5
k_θ	353.2e-6	55.1e-6
k_β	117.4e-6	83.1e-6
c_z	0.47e-3	0.35e-3
c_θ	1.1e-9	0.44e-9
c_β	0.51e-9	0.43e-9
x_d	0	-0.603e-3
y_d	0	0.0

TABLE 2 Steady Flying Attitudes for 3.5 gram loadand FH for 3.0 gram load

Radii ,Skew) (mm, deg)	FH_{RW} (nm)	FH_{min} (nm)	Pitch (μrad)	Roll (μrad)	FH_{RW} (nm) for 3.0 gram
46.0 (17.0^{o})	25.48	18.21	309.2	-1.54	31.60
33.6 (6.5^{o})	25.57	27.86	207.4	9.09	30.04
21.2 (-7.5^{o})	25.45	20.45	116.3	-6.10	27.91

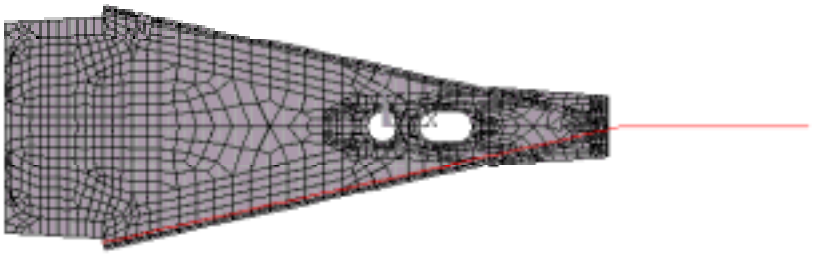

Fig. 1 Suspension model for L/UL simulation

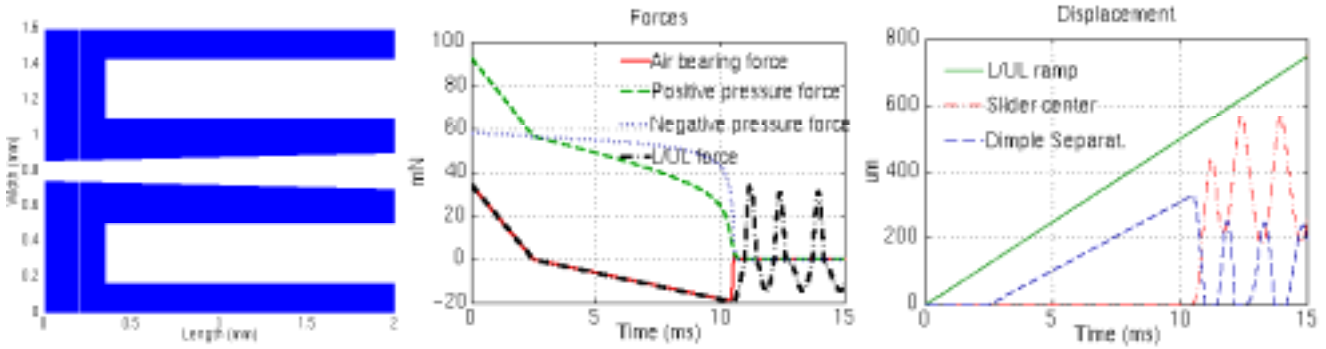

a) Type A

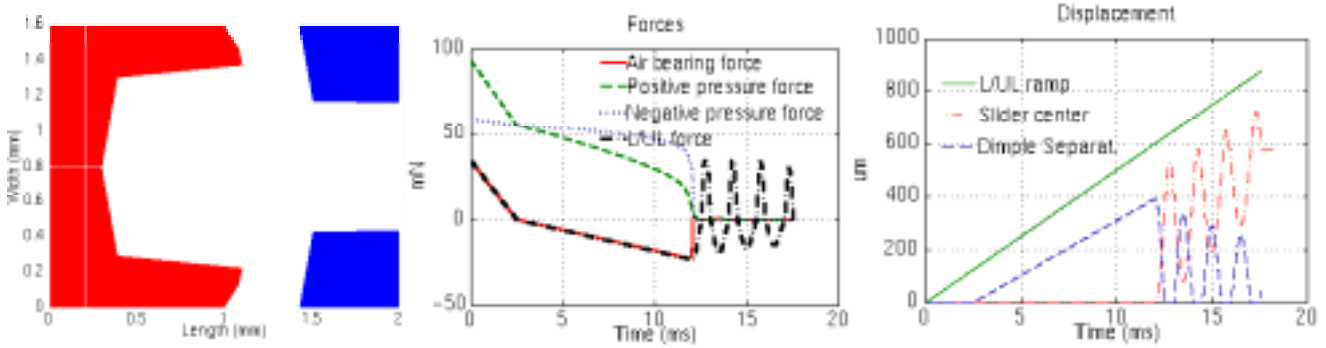

b) Type B

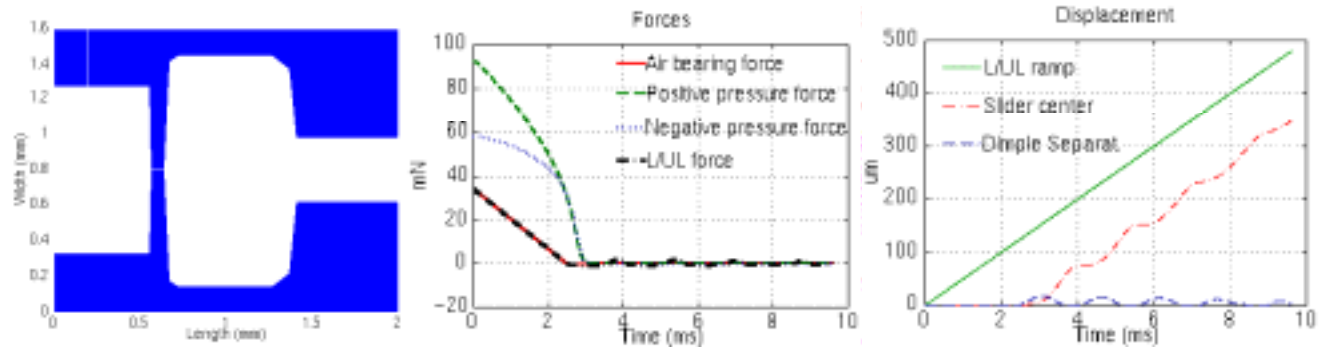

c) Type C

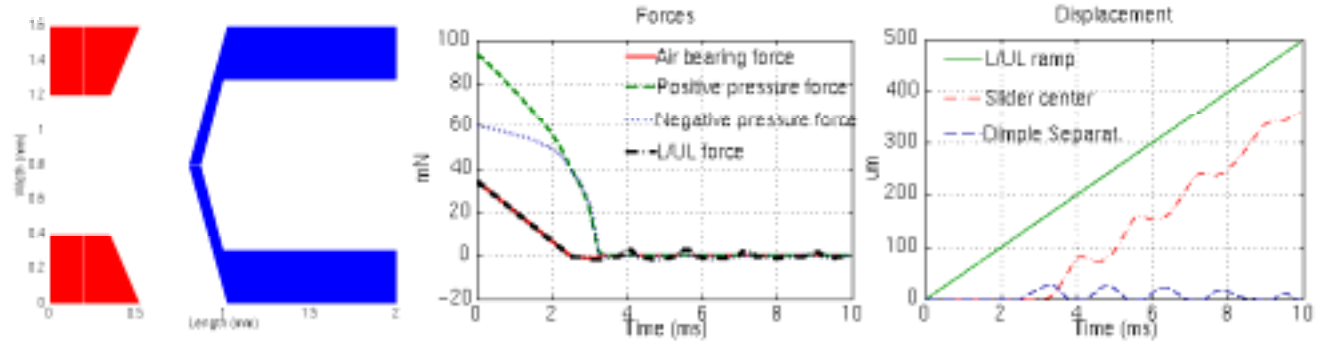

d) Type D

Fig. 2 Four basic types of ABS designs (rail shapes, force and displacement histories during unload at the OD, 5400 disk RPM, and 50 mm/s unload speed)

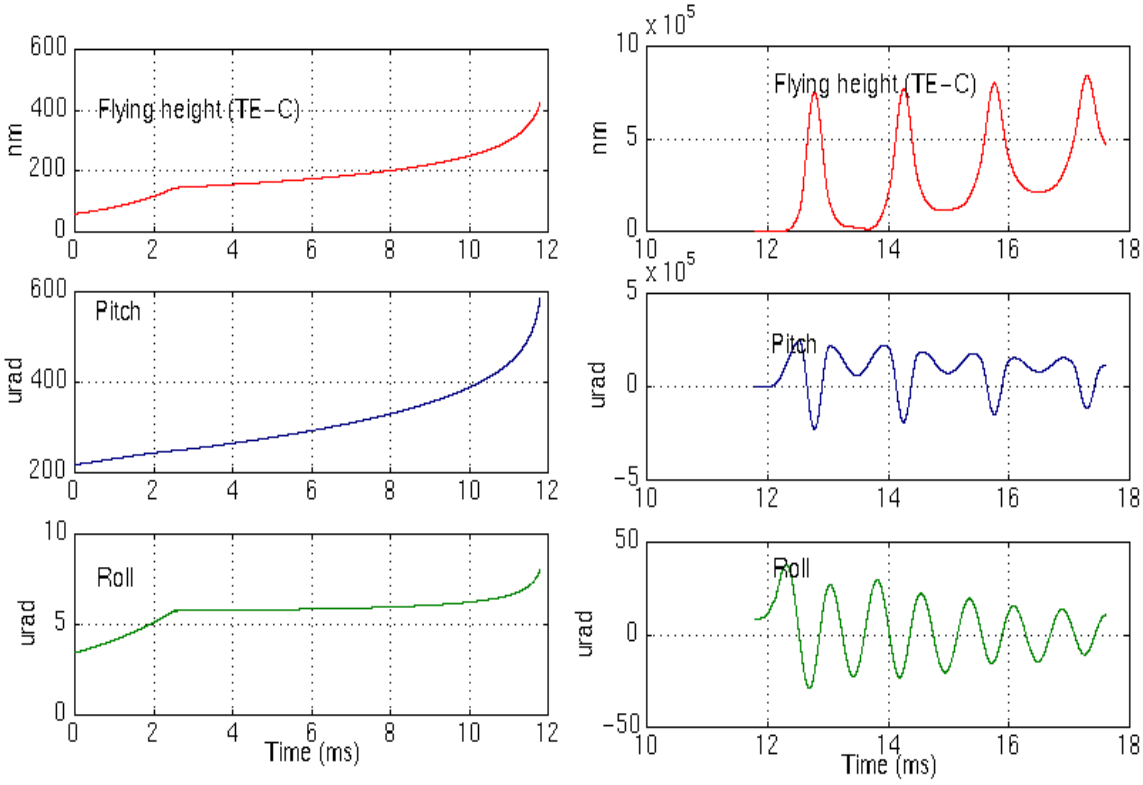

a) Stages 1 and 2 b) Stages 3 and 4

Fig. 3 Flying attitudes of the Type B slider during unload

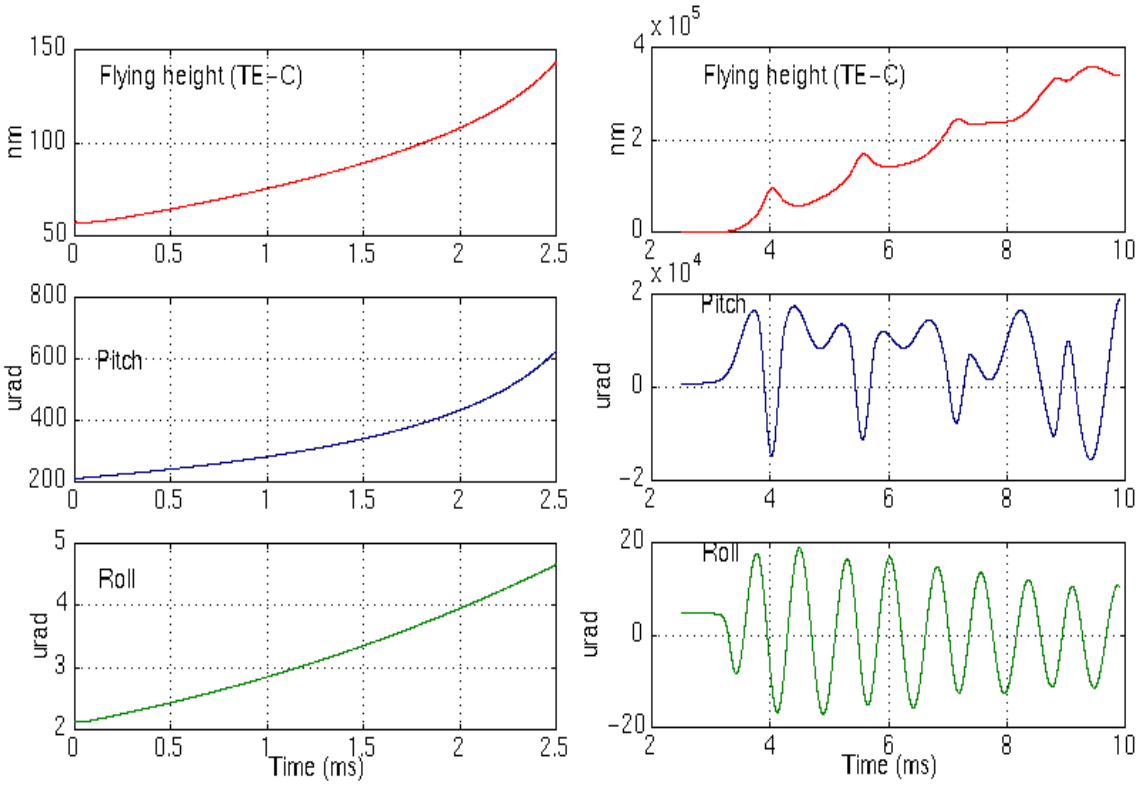

c) Stage 1 b) Stages 3 and 4

Fig. 4 Flying attitudes of the Type D slider during unload

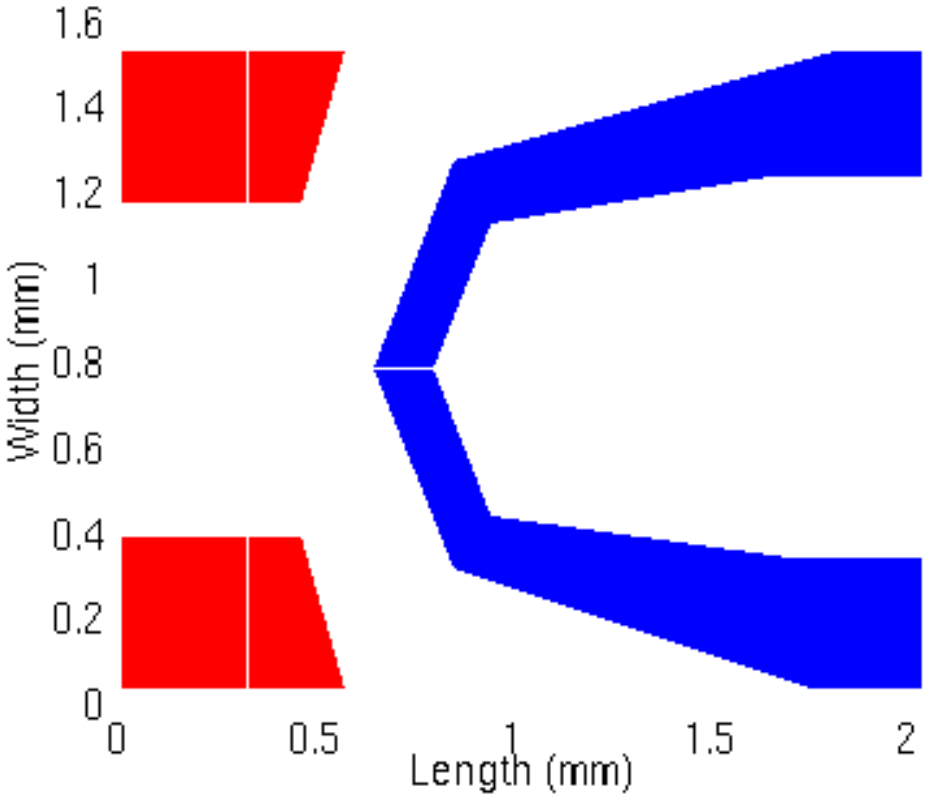

Fig. 5 A slider specifically designed for L/UL application

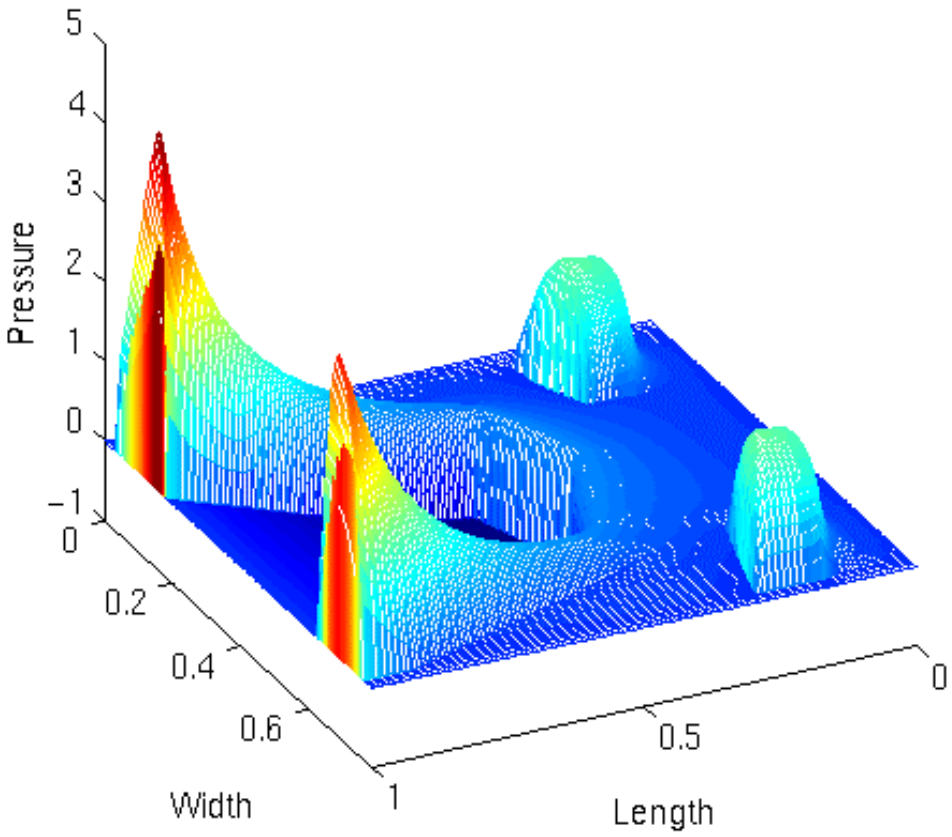

Fig. 6 Pressure profile at the ID

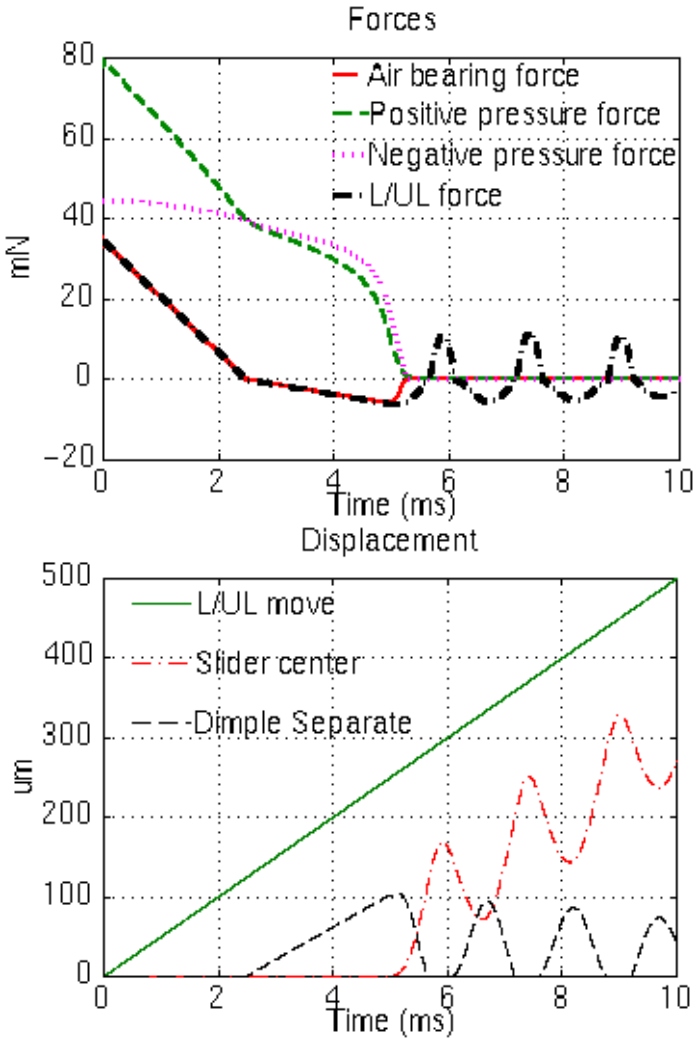

Fig. 7 Force and displacement histories during unload at 2000 RPM

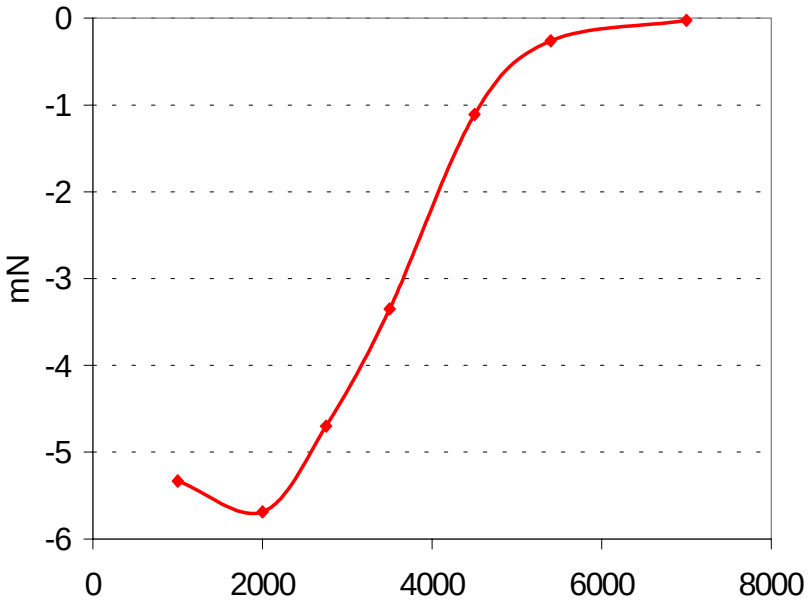

Fig. 8 Lift-off forces vs disk RPMs

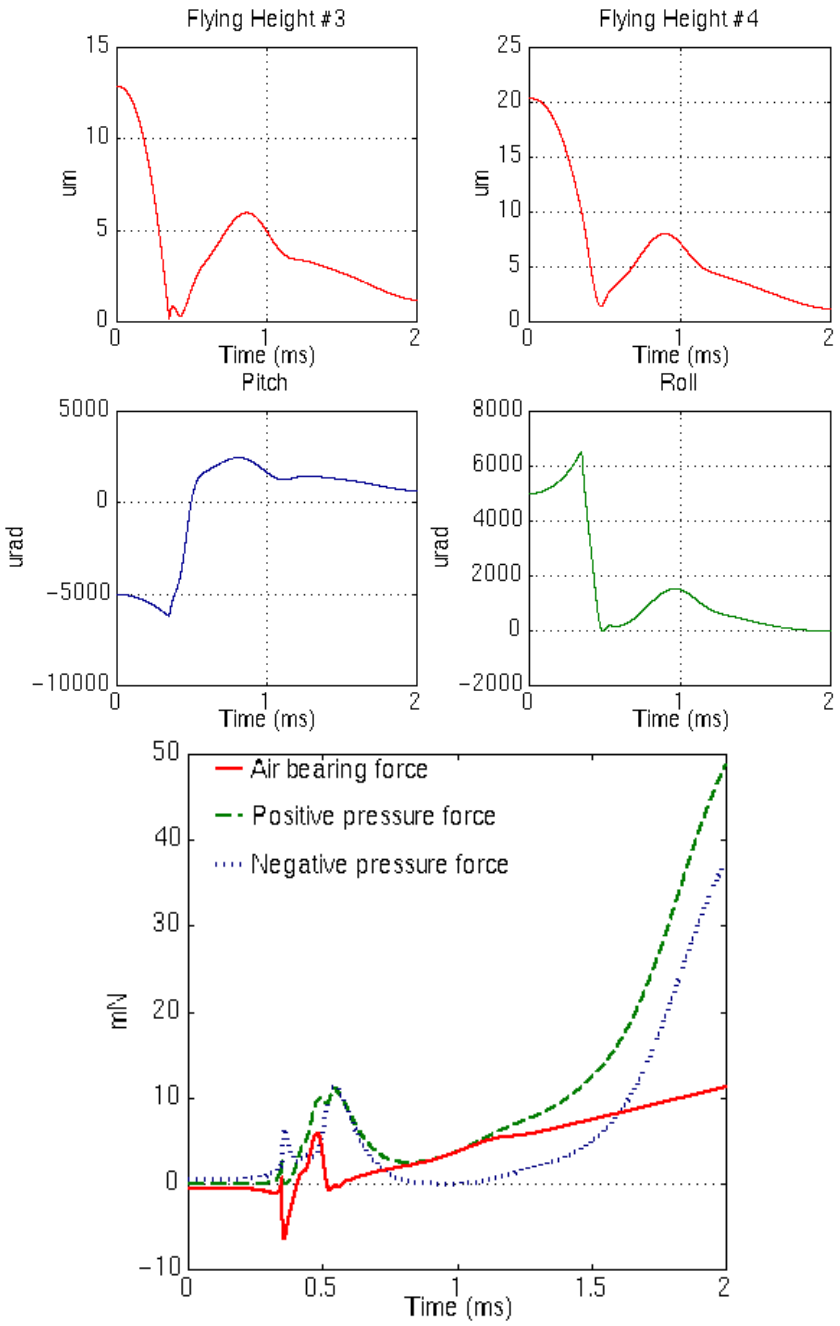

Fig. 9 Flying attitudes and force histories during load at 5400 RPM

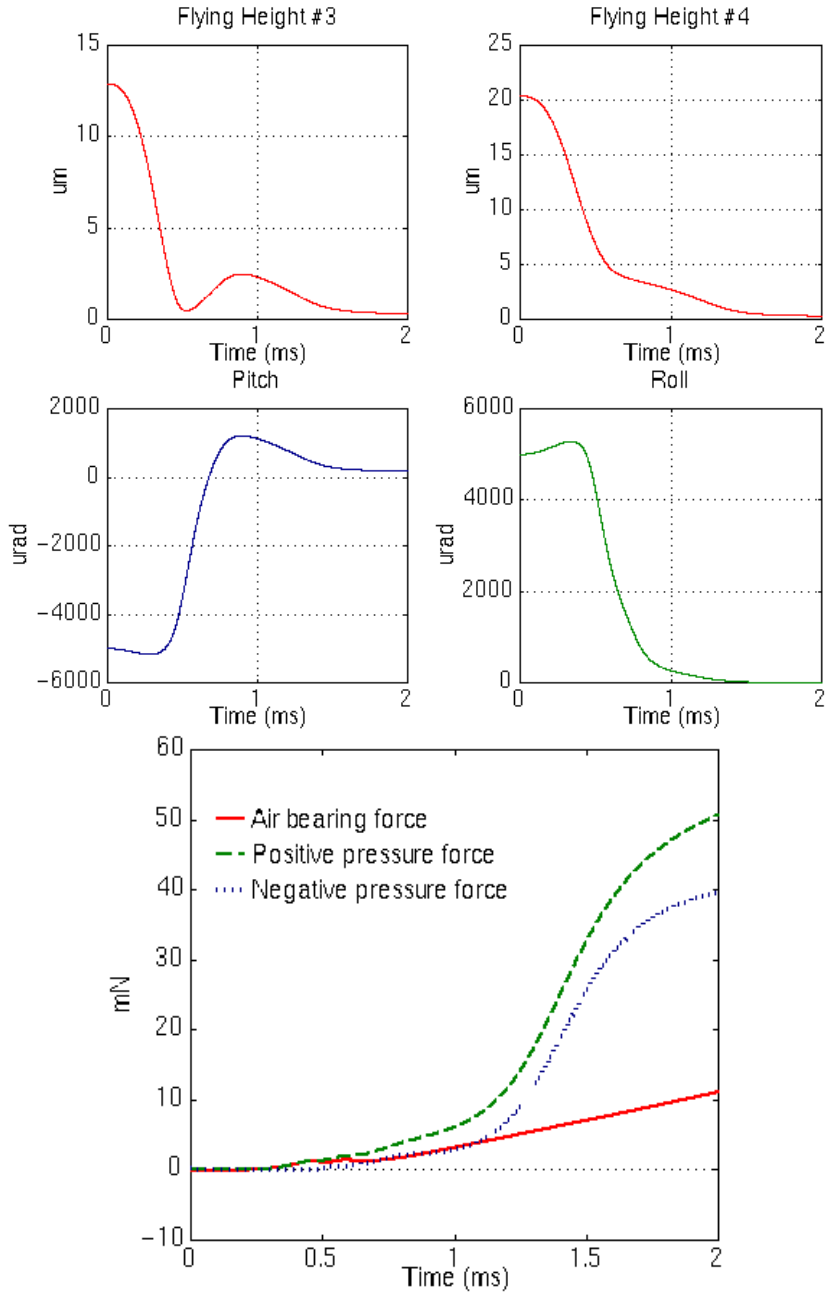

Fig. 10 Flying attitudes and force histories during load at 2000 RPM

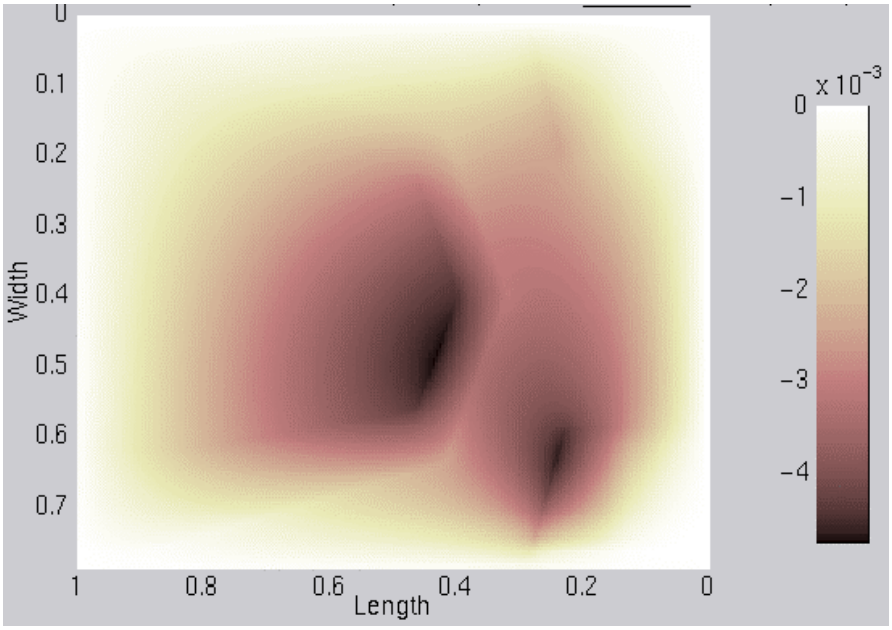

Figure 11 Prossure profile at 5400 RPM, -5mrad pitch, 5 mrad roll, and 25 um at the slider center

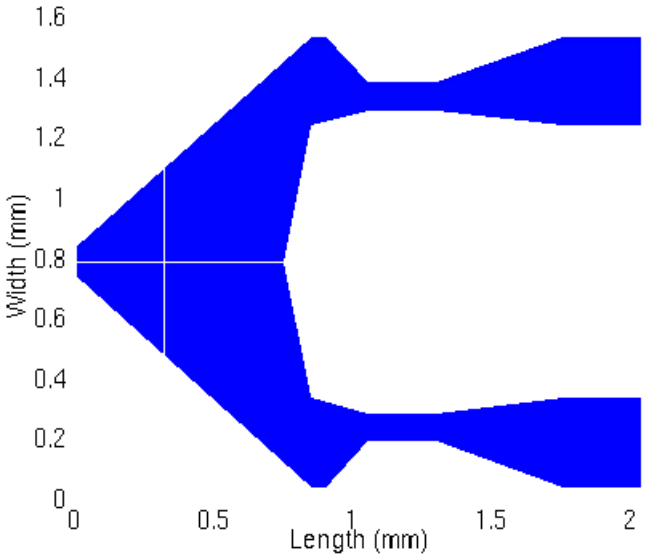

Fig. 12 A slider with better load performance